

ON THE NATURE OF SODIUM EXCESS OBJECTS. I. DATA AND OBSERVED TRENDS

HYUNJIN JEONG¹, SUKYOUNG K. YI² JAEMANN KYEONG¹, MARC SARZI³, EON-CHANG SUNG¹, AND KYUSEOK OH²

¹Korea Astronomy and Space Science Institute, Daejeon 305-348, Korea; hyunjin@kasi.re.kr

²Department of Astronomy & Yonsei University Observatory, Yonsei University, Seoul 120-749, Korea; yi@yonsei.ac.kr

³Centre for Astrophysics Research, University of Hertfordshire, Hatfield AL10 9AB, UK

Draft version October 31, 2018

ABSTRACT

Several studies have reported the presence of sodium excess objects that have neutral atomic absorption lines at 5895 Å (NaD) and 8190 Å that are deeper than expected based on stellar population models that match the stellar continuum. Their origin is therefore hotly debated. van Dokkum & Conroy proposed that low-mass stars ($\lesssim 0.3 M_{\odot}$) are more prevalent in massive early-type galaxies, which may lead to a strong NaI 8190 line strength. It is, however, necessary to test this prediction against other prominent line indices in optical wavelengths such as NaD, Mg *b* and Fe 5270, which are measurable with a significantly higher signal-to-noise ratio than NaI 8190. We newly identified roughly a thousand NaD excess objects (NEOs, $\sim 8\%$ of galaxies in the sample) based on the NaD line strength in the redshift range $0.00 \leq z \leq 0.08$ from the Sloan Digital Sky Survey (SDSS) DR7 through detailed analysis of galaxy spectra, and then explored their properties. The novelty of this work is that galaxies were carefully identified through direct visual inspection of SDSS images, and we systematically compared the properties of NEOs and those of a control sample of normal galaxies in terms of NaD line strength. Note that the majority of galaxies with high velocity dispersion ($\sigma_e > 250 \text{ km s}^{-1}$) show NaD excess. Most late-type NEOs have strong H β line strengths and significant emission lines, which are indicative of the presence of young stellar populations. This implies that the presence of interstellar medium (ISM) and/or dust contributes to the increase in NaD line strengths observed for these galaxies, which is in good agreement with the earlier study of Chen et al. who used the NaD line index to study outflow activity in star-forming disk galaxies. In contrast, the majority of *early-type* NEOs are predominantly luminous and massive systems, which is in agreement with the findings of van Dokkum & Conroy. However, we find that models used to reproduce the NaI 8190 line strengths that adopt a bottom-heavy initial mass function (IMF) are *not* able to reproduce the observed NaD line strengths. By comparing the observed NaD, Mg *b* and Fe 5270 line strengths with those of the models, we identify a plausible range of parameters that reproduce the observed values. In these models, the majority of early-type NEOs are “ α -enhanced” ($[\alpha/\text{Fe}] \sim 0.3$), “metal-rich” ($[\text{Z}/\text{H}] \sim 0.3$) and especially “Na-enhanced” ($[\text{Na}/\text{Fe}] \sim 0.3$). Enhanced Na abundance is a particularly compelling hypothesis for the increase in the strength of the NaD line index in our early-type NEOs that appear devoid of dust, both in their SDSS images and spectra.

Subject headings: catalogs – galaxies: elliptical and lenticular, cD – galaxies: spiral – galaxies: abundances – galaxies: stellar content – galaxies: evolution

1. INTRODUCTION

Deciphering galaxy spectra is important to understand the formation and evolution of galaxies. Prominent absorption features of galaxy spectra are widely used to study galaxy properties, because they reflect the average surface gravities, effective temperatures and metallicities of stellar components.

The behavior of spectral features in some galaxies in terms of sodium has received much attention as it has become known that some galaxies show enhanced NaD doublet strengths at 5890 and 5896 Å and NaI 8190 doublet strengths at 8183 and 8195 Å.

NaD index is one of the strong absorption features of optical spectra, while NaI 8190 is one of the most prominent features in the near-IR (NIR) spectral range. Numerous studies have been performed over the last three decades to understand these lines. It is now generally recognized that these lines are affected by the choice of an initial mass function (IMF), because these lines are strong in stars with a mass of less than $0.3 M_{\odot}$. However, it is important to keep in mind that the NaD feature is

more sensitive to Na-enhancement ($[\text{Na}/\text{Fe}]$) than gravity, and it can also be affected by the interstellar medium (ISM). Furthermore, both NaD and NaI 8190 absorption features are sensitive to age and metallicity.

What, then, causes NaD excess objects (hereafter NEOs)? The mechanism of NaD excess has been debated. One of the leading hypotheses is that NaD excess is related to the ISM, even though it is unclear what the dominant process is: galactic-scale gaseous outflows (galactic wind) in actively star-forming galaxies or active galactic nucleus (AGN) activity. It is well known that galactic winds are ubiquitous in star-forming galaxies (Heckman, Armus & Miley 1990), and Chen et al. (2010) argued that NaD absorption arises from cool gas in the disk, which is entrained in galactic wind. In contrast, Lehnert et al. (2011) investigated the properties of NaD line strengths in a sample of radio galaxies and concluded that AGN activity plays an important role in powering the outflow/heating phase of the feedback cycle.

Another candidate is metal abundance. The discov-

ery of non-solar abundance patterns in early-type galaxies was first made by O’Connell (1976) and Peterson (1976). They found extreme enhancement of Mg *b* and Na D features with respect to calcium and iron peaks, and concluded that this was a result of a higher metal abundance. Later, Carter, Visvanathan & Pickles (1986) measured the Na I, Ca II triplet, TiO and FeH features of 14 early-type galaxies and confirmed that these features are associated with metal abundance (see also Alloin & Bica 1989). Worthey (1998) also claimed that strong Na features are caused by an overabundance of [Na/Fe] (see also Worthey, Ingermann & Serven 2011).

The latest compelling mechanistic theory is that of variation of the IMF. The stellar IMF is usually considered a universal function, but the possibility of a non-universal IMF has been raised by several authors (see e.g. Davé 2008; van Dokkum 2008; Trager et al. 2000; Graves, Faber & Schiavon 2009; Treu et al. 2010; van Dokkum & Conroy 2010). One of the first observational attempts to constrain the low-mass portion of the IMF was made by Spinrad & Taylor (1971). They compared the observed line strengths of some IMF sensitive lines such as Na I and TiO in the centers of M31, M32 and M81 with the population synthesis models and claimed a substantial fractional contribution by dwarf stars to the integrated light of galaxies. Cohen (1978) also measured the strengths of Na I 8190 and TiO in the centers of M31 and M32 and concluded that the IMF is equal to that of the Galactic disk. However, Faber & French (1980) argued for a bottom-heavy (dwarf-rich) IMF, despite the fact that their results were also based on the Na I 8190 line strengths in M31 and M32. Indeed, it is a challenge to estimate the number of low-mass stars from an integrated spectrum, because low-mass stars are too faint to have a strong influence on the integrated spectrum.

The debate over IMF variation, however, was reopened by Saglia et al. (2002). They found an anti-correlation between the strength of the Ca II triplet region at 8500 Å and velocity dispersion for elliptical galaxies and concluded that bottom-heavy IMFs are favored (see also Cenarro et al. 2003). Recently, van Dokkum & Conroy (2010) reported observing the near-infrared Na I 8190 doublet in the spectra of massive early-type galaxies, and claimed that this excess can be explained by the bottom-heavy IMF (see also van Dokkum & Conroy 2012). If correct, massive early-type galaxies should possess relatively more low-mass stars, and this would affect the mass-to-light ratio (M/L) of galaxies. Cappellari et al. (2012) claimed that there was systematic variation in the IMF in early-type galaxies as a function of stellar M/L ratios based on detailed dynamical modeling of ATLAS^{3D} early-type galaxies (see e.g. Cappellari et al. 2011), but the expected maximum slope of the IMF is about 2.8 ($x \sim -2.8$), which is lower than that proposed by van Dokkum & Conroy (2010), and there are many high velocity dispersion galaxies that prefer a Salpeter IMF (Salpeter 1955).

Three origins of Na D excess have been hypothesized: (1) the ISM, (2) metallicity and (3) a bottom-heavy stellar IMF. To determine which of the above is correct, we explore the properties of NEOs in the redshift range $0.00 \leq z \leq 0.08$ from the seventh data release of the Sloan Digital Sky Survey (SDSS; Abazajian et al. 2009), with

TABLE 1
SUMMARY OF SAMPLING CRITERIA

Criterion	Explanation
$0.00 \leq z \leq 0.08$	Limit redshift for morphological classification
$M_r < -20.5$	The absolute r-band magnitude cut for a volume-limited sample
$S/N > 20$	Guarantee the quality of spectroscopic data
$rN/sN^a \leq 1.5$	Guarantee the quality of the fit to the stellar continuum

Notes.

^aOh et al. 2011

spectral measurements retrieved from Oh et al. (2011). Almost all previous studies have focused on either early-type or late-type galaxies. However, it is important to investigate Na D excess according to galaxy morphology. The novelty of this paper is that we simultaneously inspect images to identify the morphology of galaxies and explore the photometric and spectroscopic properties of sample galaxies based on homogeneous data sets. Therefore, the catalogue presented here is a useful reference sample of NEOs with morphological information.

In this paper, we focus on the Na D feature of galaxies. In Section 2, we briefly summarize the photometric and spectroscopic data and describe the sample and our method for selecting NEOs. The properties of early-type and late-type NEOs are presented in Sections 3 and 4, respectively. Finally, we discuss the origin of NEOs in Section 5.

2. DATA CONSTRUCTION

2.1. Sloan Digital Sky Survey (SDSS) and OSSY Catalogue

SDSS has established the largest and most homogeneous database of both photometric (u , g , r , i and z bands) and spectroscopic data for about one million galaxies. However, it is known that the SDSS pipeline spectroscopic data measurements still have a few crucial defects. The most serious problem is that the pipeline values for the absorption line strength are contaminated with nebular emissions. Oh et al. (2011, hereafter OSSY) recently released new and improved absorption and emission-line measurements for the SDSS galaxies using the Gas AND Absorption Line Fitting routine (GANDALF; Sarzi et al. 2006) and the penalized pixel-fitting code (pPXF; Cappellari & Emsellem 2004). Furthermore, they provided information about the best-fit models for the SDSS spectra. We start the analysis based on this OSSY catalogue.

We obtain photometric values from the Catalog Archive Server for DR7. Note that we use Petrosian and model magnitudes to estimate galaxy luminosities and colors, respectively. We also deredden the colors with respect to Galactic extinction using dust maps provided by the SDSS pipeline (Schlegel et al. 1998) and apply a k -correction based on simple two-population (young plus old) modeling of the observed optical colors. Details of the k -correction are described more fully in Section 3 of Yi et al. (2012).

2.2. Sample Selection

We begin by selecting all sample galaxies with spectra in the redshift range $0.00 \leq z \leq 0.08$ and apply the absolute r-band magnitude cut-off of -20.5 to obtain a volume-limited sample. Furthermore, only galaxies with a signal-to-noise (S/N) ratio above 20 and a quality assessment value based on continuum fit (rN/sN , see section 3 of OSSY) below 1.5 are included in our sample to guarantee high quality spectroscopic data and model fit to the stellar continuum. The total number of galaxies in our sample is 20571. Our selection criteria are summarized in Table 1.

2.3. Measurement of NaD Excess

To find NEOs, we define a new index, $fNaD$, which quantifies the NaD excess as follows:

$$fNaD = \frac{NaD(\text{Observed}) - NaD(\text{Model})}{NaD(\text{Model})}, \quad (1)$$

where $NaD(\text{Observed})$ is the observed NaD line strength and $NaD(\text{Model})$ is the expected model NaD line strength. For example, a $fNaD$ value equal to 1 indicates that the observed absorption strength of NaD is two times stronger than that expected for the best-fit model. Details of the continuum fitting and absorption line measurements are described in OSSY, so we only briefly summarize the process here. The OSSY team first separated the contributions of the stellar continuum and ionized-gas emission to the observed spectrum by matching them only for emission-free regions using a set of stellar templates. They then measured the emission-line strengths by fitting the stellar templates and Gaussian emission-line templates to the data. During this process, they used both the stellar population synthesis models of Bruzual & Charlot (2003) and the MILES stellar templates (Sánchez-Blázquez et al. 2006), and calculated internal reddening due to dust (see Section 3.5 for details). Finally, they subtracted the emission-line spectrum from the observed one to get the clean absorption line spectrum, and then measured the absorption line indices from this cleaned spectrum following standard line-strength index definitions.

In Figure 1, we plot the distribution of $fNaD$ for a total of 20571 galaxies. Interestingly, the distribution is skewed with a tail toward higher values. We fit a Gaussian curve to the NaD excess index distribution and plot it using the red dot-dashed line to dramatize the presence of NEOs. Moreover, the peak (vertical solid line) in the distribution does not correspond to zero. In other words, more galaxies tend to have positive $fNaD$ values.

We adopt a conservative limit of $fNaD = 0.5$ to pick out galaxies showing NaD excess. This demarcation for identifying NEOs ($fNaD \geq 0.5$) is indicated by the vertical dashed line in Figure 1. The overall fraction of NEOs within our criterion is roughly 7.8% (1603/20571). Interestingly, NaD deficient objects (NDO) also exist. If we adopt a limit of $fNaD = -0.5$ (vertical dotted line) to select NDOs ($fNaD \leq -0.5$), the overall fraction of NDOs is about 0.6% (120/20571). We note that most NDOs are strong emission-line galaxies. Bica & Alloin (1986) indeed reported that a few late-type galaxies have a NaD emission line. This implies that the NaD absorption feature can be affected by the NaD emission line, and that continuum fits may be influenced by emission lines.

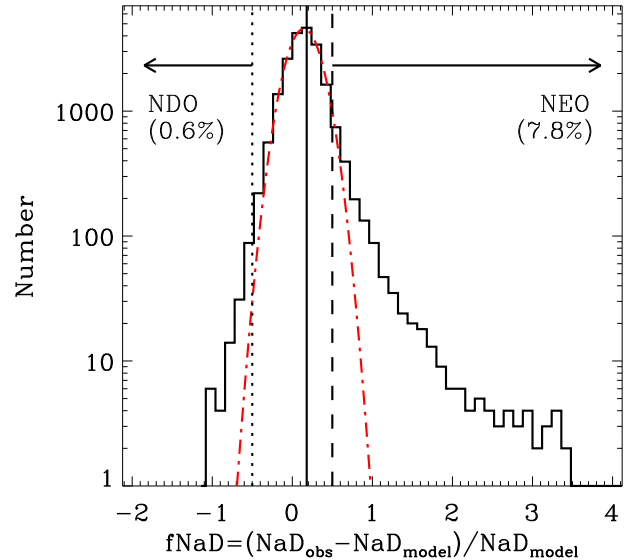


FIG. 1.— Distribution of $fNaD$. The peak value is shown by the black solid line. The red dot-dashed line is a Gaussian fit to the data. From the total sample of 20571 galaxies, we selected a subsample of 1603 galaxies with significant NaD excess ($fNaD \geq 0.5$, dashed line). Note that NaD deficient objects (NDO) also exist ($fNaD \leq -0.5$, dotted line). A color version of this figure is available in the online journal

TABLE 2
RESULTS OF MORPHOLOGICAL CLASSIFICATION

Classification	Number
Control Sample (1036)	
Early-type galaxies	694
Late-type galaxies	342
NEOs (963)	
oETG ^a	206
pETG ^b	347
oLTG ^c	56
pLTG ^d	354

Notes.

^aordinary early-type NaD excess objects

^bpeculiar early-type NaD excess objects

^cordinary late-type NaD excess objects

^dpeculiar late-type NaD excess objects

An important objective of this paper is a systematic comparison of the properties of NEOs and those of a control sample of galaxies that do not show NaD excess. We create a control sample of ~ 1600 galaxies in the NaD excess range $0.0 \leq fNaD \leq 0.1$, based on the pick value of $fNaD$ of about 0.1 (see Figure 1). The classification scheme is summarized below:

$$\begin{aligned} fNaD \geq 0.5 & \quad \text{NaD excess objects (NEOs)} \\ 0.0 \leq fNaD \leq 0.1 & \quad \text{Control sample} \\ fNaD \leq -0.5 & \quad \text{NaD deficient objects (NDOs)} \end{aligned} \quad (2)$$

Observed stacked spectra (black solid lines) of sample galaxies with their stacked best fits (red dot-dashed lines), normalized at 5800 \AA , are shown in Figure 2. We construct the stacked galaxy spectra by selecting ~ 300 early-type looking galaxies in the $fNaD$ range $0.0 \leq fNaD \leq 0.1$ (for the control sample) and $fNaD \geq 0.5$ (for the NEOs), respectively, and we also estimate the 1σ

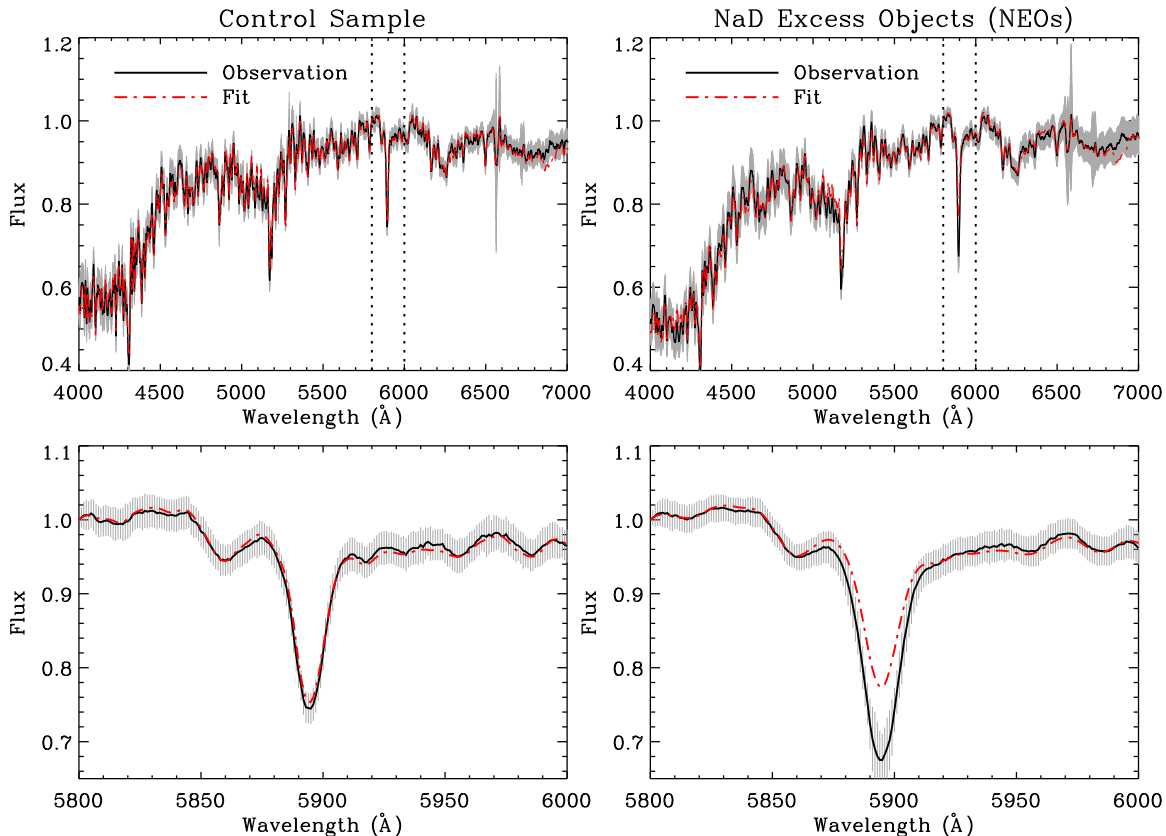


FIG. 2.— Sample SDSS stacked spectra of our control sample galaxies and NaD excess objects. The observed spectra, including the 1σ scatter, are shown by the black solid lines, together with their best fits (red dot-dashed lines). The bottom figures show the spectra in the regions of the NaD feature. The spectra were normalized at 5800 Å. A color version of this figure is available in the online journal.

scatter (grey lines). The overall observed spectra match the models well. However, there is a marked discrepancy in fit in the specific index region for sodium near 5900 Å. The vast majority of the spectra are well matched (left), but some galaxies (NEOs, $\sim 7.8\%$) show a much stronger observed line index than expected based on the best-fit model (right). We note that the expected model NaD line strengths of the control sample and NEOs are almost the same.

2.4. Visual Classification

As the final step, we perform visual classification of the sample. Images used for morphological classification are provided by the SDSS DR7 release. The sample galaxies showing NaD excess are carefully assigned to four main classes: (1) ordinary early-type galaxies (oETGs), (2) peculiar early-type galaxies (pETGs), (3) ordinary late-type galaxies (oLTGs) and (4) peculiar late-type galaxies (pLTGs). Note that galaxies that exhibit any asymmetric features (e.g. shells and tails), dust patches or dust lanes (especially for early-type galaxies) are classified as peculiar galaxies, that is, categories (2) or (4). Our classification scheme, therefore, is to construct robust ordinary samples (categories (1) and (3)). There are, however, little differences among late-type galaxies. We use only two categories for the control sample: early-type galaxies and late-type galaxies.

Additionally, we keep the galaxy as a sample if we can precisely morphologically classify it. When we are unsure of the classification, the galaxy is classified as an

unknown galaxy. This process yields a final sample of 206 reliably classified oETGs, 347 pETGs, 56 oLTGs, 354 pLTGs, 694 early-type control samples and 342 late-type control samples. Details are listed in Table 2. Figure 3 shows a plot of the redshift distributions of NEOs and control sample galaxies. Note that we initially construct a volume-limited sample, but using an S/N cut and visual classification leads to exclusion of a fair fraction of more distant galaxies from our sample. It is also interesting to note that only 15% of galaxies that show extreme NaD excess ($f_{\text{NaD}} \geq 1.0$) are classified as early-type galaxies.

3. PROPERTIES OF EARLY-TYPE NaD EXCESS OBJECTS

3.1. Color-Magnitude Relation

The color-magnitude relation (CMR) is widely used to study the star formation history of galaxies. Galaxies are populated in three main regions of the color-magnitude diagram: the red sequence, the blue cloud and the green valley in between. It is known that the optical CMR of early-type galaxies shows a small scatter around the mean relation. In other words, almost all of the early-type galaxies are on the red sequence.

Figure 4 shows the u-r CMR. The u-r CMR is a particularly good tool for tracking the presence of young stellar populations. Grey contours, red filled circles and red open circles indicate the early-type control sample, ordinary and peculiar early-type NEOs, respectively. A cursory glance at this diagram shows that most ordinary

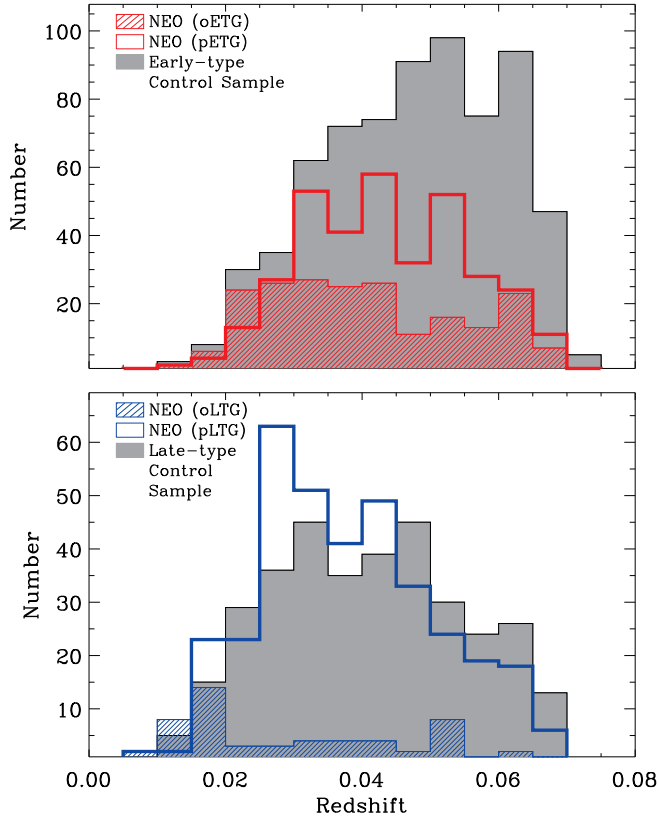


FIG. 3.— *Top*: Distribution of redshift for our visually classified ordinary (red hashed) and peculiar (red solid) early-type NEOs. The grey filled histogram represents the early-type control sample. *Bottom*: Distribution of redshift for our visually classified ordinary (blue hashed) and peculiar (blue solid) late-type NEOs. The grey filled histogram represents the late-type control sample. A color version of this figure is available in the online journal.

early-type NEOs (oETGs, filled circles) reside in the well-defined red sequence, while peculiar early-type NEOs (pETGs, open circles) have a wide color baseline. This is because our morphological classification scheme for peculiar galaxies allows for a wide variety of galaxies, ranging from dusty red galaxies to star-forming blue galaxies possessing shells, tidal features and signatures of recent star formation. The M_r and $u-r$ color distributions of the ordinary (red hashed) and peculiar (red solid) early-type NEOs compared to those of their control-sample counterparts (grey filled) are shown in Figure 4. Ordinary early-type NEOs are more luminous and optically redder than the control sample. Meanwhile, the majority of peculiar early-type NEOs are also slightly more luminous and redder than the control sample, but vary in luminosity and color.

3.2. Velocity Dispersion and Stellar Mass

Stellar velocity dispersion is one of the important physical parameters of galaxies, and can be used to estimate galaxy mass by applying the virial theorem or a related method. Because SDSS fibers have a fixed diameter, we apply aperture correction to the observed velocity dispersion using the following formula of Cappellari et al. (2006):

$$\sigma_e = \left(\frac{R_{\text{fiber}}}{R_e} \right)^{0.066 \pm 0.035} \sigma_{\text{fiber}}, \quad (3)$$

where R_{fiber} is the aperture radius of the SDSS fiber (1.5") and R_e is the effective radius.

The stellar mass of each galaxy is also derived from its color and luminosity using the following formula of Bell et al. (2003):

$$\log \left(\frac{M_*}{M_\odot} \right) = -0.306 + 1.097(g-r) - 0.4(M_{r,*} - M_{r,c}) \quad (4)$$

Figure 5 shows the stellar mass of our early-type sample as a function of velocity dispersion. Both ordinary (red filled circles) and peculiar (red open circles) early-type NEOs generally tend to have higher velocity dispersions and correspondingly bigger masses than the majority of the control sample (grey contours). We also plot the distributions of velocity dispersion and stellar mass for ordinary (red hashed) and peculiar (red solid) early-type NEOs. The histograms for the control sample (grey filled) are also provided for comparison. We find again that ordinary early-type NEOs have significantly higher velocity dispersions and are relatively more massive systems than the average early-type control sample. Furthermore, we checked the velocity dispersions of all sample galaxies in the NaD excess range $0.0 \leq f\text{NaD} \leq 0.1$ and find that only 0.5% (17/3461) of galaxies without a significant NaD excess have velocity dispersions greater than 250 km s^{-1} . This implies that the majority of high velocity dispersion galaxies show NaD excess. Our results are consistent with those of Spiniello et al. (2012) and Ferreras et al. (2013), who found a correlation between NaI 8190 line strengths and velocity dispersions. Meanwhile, peculiar early-type NEOs have a wide range of velocity dispersions.

3.3. Emission Line Diagnostics: Star Formation and AGN Activity

The ratios of emission lines can be used to distinguish various classes of emission line galaxies and ionization mechanisms. One of the most frequently used methods is the BPT diagram, proposed by Baldwin, Phillips & Terlevich (1981), on the basis of $[\text{O III}] \lambda 5007/\text{H}\beta \lambda 4861$ and $[\text{N II}] \lambda 6583/\text{H}\alpha \lambda 6563$ ratios. This method allows the classification of galaxies into star-formation-dominant and AGN-dominant galaxies.

BPT diagrams for the early-type control sample (left, black filled circles), ordinary early-type NEOs (middle, red filled circles) and peculiar early-type NEOs (right, red open circles) are shown in Figure 6. We note that galaxies in which all four emission lines are detected with an amplitude-over-noise (A/N from GANDALF, which is similar to the signal-to-noise ratio) greater than 3 are classified as either ‘star-forming’, ‘composite’ (i.e. hosting both star formation and AGN activity), ‘Seyfert’ or ‘LINER’ using the demarcation lines of Kauffmann et al. (2003, dashed curve), Kewley et al. (2001, 2006, solid curve) and Schawinski et al. (2007, straight line). Galaxies without a detection in all four lines are classified as ‘quiescent’ galaxies. Details are provided in Table 3.

Early-type NEOs exhibit a two-fold higher fraction of strong emission lines ($\sim 21\%$) than the early-type control sample ($\sim 11\%$). Moreover, the fraction of early-type NEOs classified as ‘star-forming’ is four-fold that

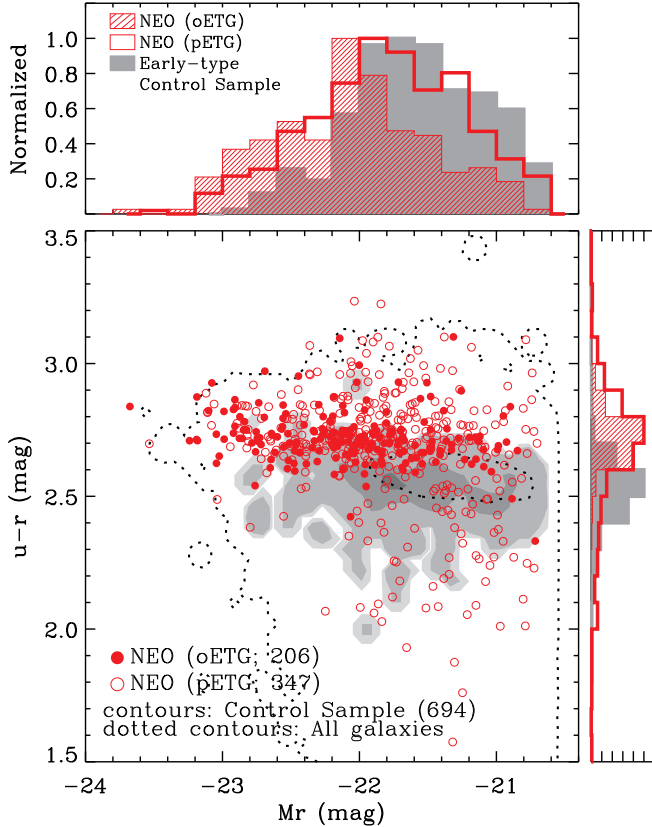


FIG. 4.— *Top*: Distribution of r -band absolute magnitudes for our early-type sample. The grey filled histogram represents the early-type control sample, while the red hashed and solid histograms indicate the ordinary (oETGs) and peculiar (pETGs) early-type NaD excess objects. *Bottom-left*: Color-magnitude relation for our early-type NaD excess objects. The ordinary (oETGs) and peculiar (pETGs) early-type NEOs are plotted as red filled and open circles, respectively. The contours of the early-type control sample (grey shaded) and all sample galaxies (dotted) are shown for comparison. *Bottom-right*: Distribution of $u-r$ colors for our early-type sample. A color version of this figure is available in the online journal.

of the control counterpart. The reason why early-type NEOs show a higher fraction of strong emission lines is mainly because of peculiar early-type NEOs. Most ordinary early-type NEOs are virtually free of emission lines ($\sim 91\%$). It is also worth noting that the overwhelming bulk of emission in ordinary early-type NEOs is ‘LINER’ AGN, which implies that ordinary early-type NEOs do not host both active star formation and powerful AGNs.

3.4. Absorption Line Strengths

Spectral line strengths have been used to understand the physical processes governing the evolution of galaxies because they reflect the average surface gravities, effective temperatures and metal abundances of galaxies.

We first check whether the observed spectra match the models in specific index regions for $Mg\ b$, Fe 5270 and $H\beta$ by comparing the observed and expected model absorption strengths. The bottom three panels of Figure 7 show the $Mg\ b$ (left, $fMg\ b$), Fe 5270 (middle, $fFe\ 5270$) and $H\beta$ (right, $fH\beta$) excess indices, which are calculated using the same procedure as in formula (1), against the NaD excess index $fNaD$. The contours of the early-type control sample (grey shaded) and all sample galaxies

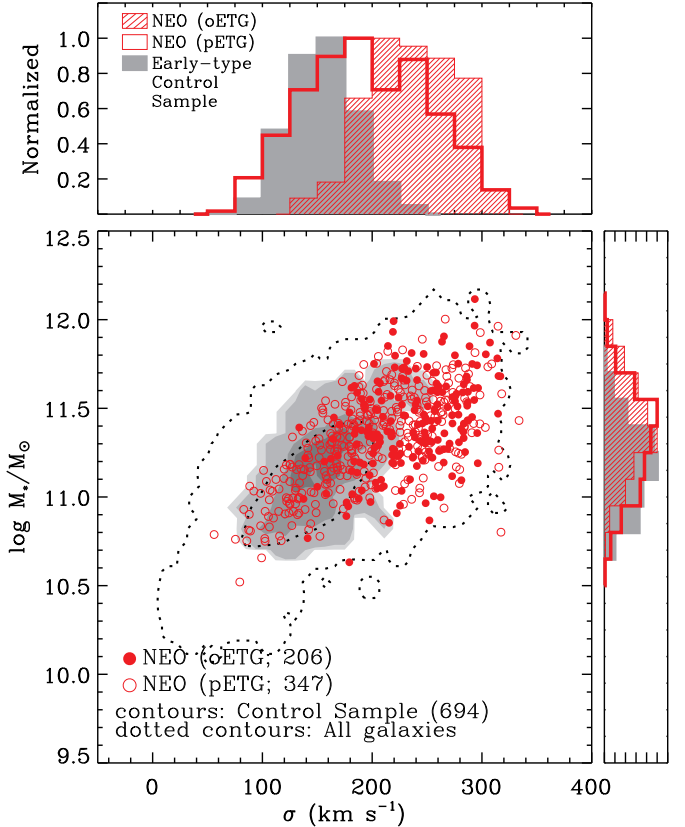


FIG. 5.— *Top*: Distribution of velocity dispersions for our early-type sample. Early-type control sample, ordinary and peculiar early-type NEOs are represented as grey filled, red hashed and red solid histograms, respectively. *Bottom-left*: Stellar mass of our early-type NaD excess objects as a function of velocity dispersion. The ordinary early-type NEOs are shown using red filled circles, while peculiar early-type NEOs are plotted as red open circles. The contours of the early-type control sample (grey shaded) and all sample galaxies (dotted) are shown for comparison. *Bottom-right*: Distribution of stellar masses for our early-type sample. A color version of this figure is available in the online journal.

(dotted) are shown for comparison. The top panels of Figure 7 show the distributions of $fMg\ b$, $fFe\ 5270$ and $fH\beta$, respectively.

The early-type control sample and NEOs have very similar distributions of Fe 5270 and $H\beta$ excess indices, and these distributions are Gaussian, unlike $fNaD$ (see Figure 1). However, there is mismatch in the $Mg\ b$ excess index between the observed and expected model strengths, especially for ordinary early-type NEOs (red hashed histogram and red filled circles). This $Mg\ b$ excess in ordinary early-type NEOs indicates that for these galaxies, a mechanism to explain both the NaD and $Mg\ b$ excesses is required, while $fMg\ b$ is much smaller than $fNaD$. For reference, the median values of $fNaD$, $fMg\ b$, $fFe\ 5270$ and $fH\beta$ for our early-type control sample are 0.06 ± 0.03 , 0.07 ± 0.08 , -0.05 ± 0.10 and 0.0 ± 0.10 , whereas those for ordinary early-type NEOs are 0.58 ± 0.13 , 0.26 ± 0.11 , -0.06 ± 0.08 and -0.06 ± 0.09 , respectively.

We now turn to the line strength itself. Strong Balmer absorption lines (e.g. $H\beta$) betray the presence of young stars, while a combination of $Mg\ b$ and Fe 5270 yields information about the mean metallicity of the popula-

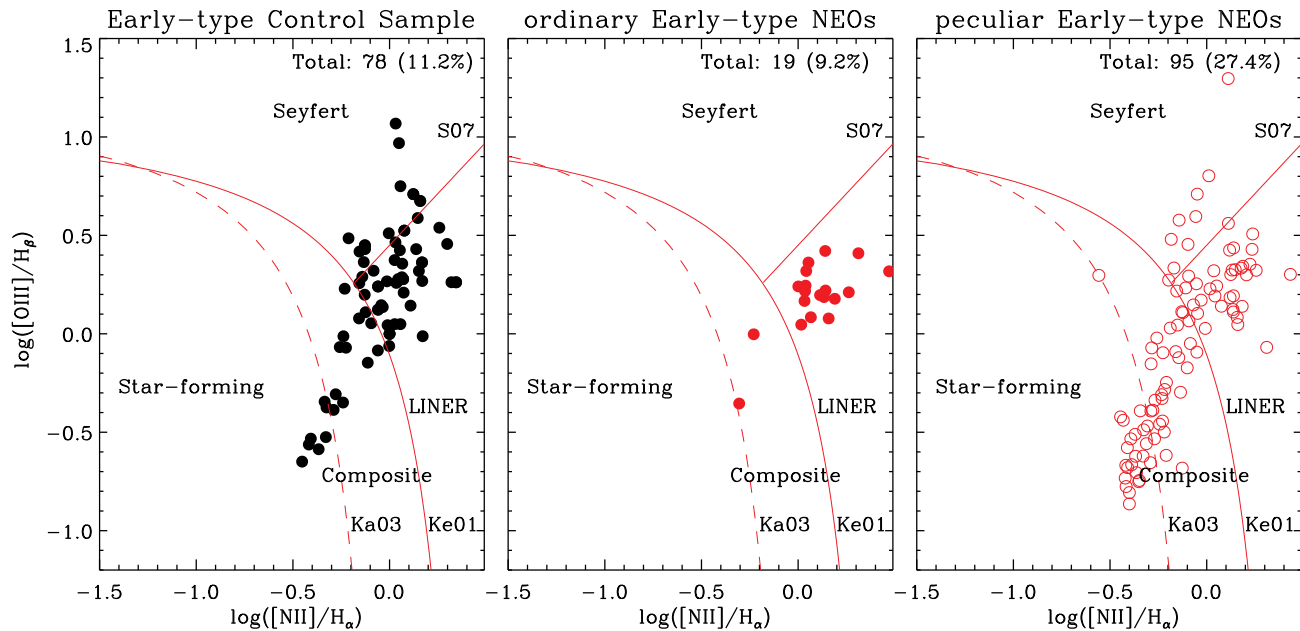


FIG. 6.— Emission-line ratio diagram for our early-type sample. Only galaxies with an A/N greater than 3 for all four lines are shown. The curve labeled Ka03 is the empirical purely star-forming limit of Kauffmann et al. (2003), while the curve labeled Ka01 is the theoretical maximum starburst model of Kewley et al. (2001). The straight line labeled S07 from Schawinski et al. (2007) divides Seyferts and LINER AGNs. Black filled circles indicate the early-type control sample (left). Ordinarily early-type NEOs are shown using red filled circles (middle), while peculiar early-type NEOs are plotted as red open circles (right). A color version of this figure is available in the online journal.

TABLE 3
RESULTS OF SPECTRAL LINE CLASSIFICATION FOR EARLY-TYPE GALAXIES

Classification	early-type control sample	early-type NEO	oETGs ^a	pETGs ^b
Quiescent	88.8% (616)	79.4% (439)	90.8% (187)	72.6% (252)
Strong emission	11.2% (78)	20.6% (114)	9.2% (19)	27.4% (95)
Star-forming	1.0% (7)	4.0% (22)	0.0% (0)	6.3% (22)
Composite	2.0% (14)	5.8% (32)	1.0% (2)	8.7% (30)
Seyfert	2.2% (15)	1.4% (8)	0.0% (0)	2.3% (8)
LINER	6.0% (42)	9.4% (52)	8.2% (17)	10.1% (35)

Notes.

^aordinary early-type NaD excess objects

^bpeculiar early-type NaD excess objects

tion. In Figure 8, we show a comparison of $fNaD$ and the line strength indices of Na D (left), Mg b (middle) and Fe 5270 (right). The NaD excess index $fNaD$ correlates strongly with the NaD line strength. This implies that NEOs are simply NaD strong galaxies. This may occur because the best-fit models for early-type NEOs generally expect NaD line strengths of around 3.0 to 3.5 Å. Therefore, these galaxies have stronger NaD line strengths and higher Na D excesses. In contrast, the Mg b and Fe 5270 line strengths do not show significant correlations with $fNaD$ due to contamination by peculiar early-type NEOs. Peculiar early-type NEOs show a wide range of Mg b and Fe 5270 values, often much lower values than those of the early-type control sample. We note that some peculiar early-type NEOs with $fNaD \geq 1$ have significantly weaker Mg b and Fe 5270 line strengths than the early-type control sample. These features are similar to late-type NEOs, as discussed in Section 4 below.

In the top panels of Figure 8, histograms of the Na D, Mg b and Fe 5270 line strengths are shown. Peculiar early-type NEOs had skewed distributions with a tail

toward lower values for Mg b and Fe 5270. Their Mg b and Fe 5270 strengths are similar to those of late-type galaxies. If some peculiar early-type galaxies have recently formed stars that are centrally concentrated, they would show similar line strength distributions to late-type galaxies because SDSS fibers encompass only central regions.

Line strength index diagrams comparing NaD, Mg b , Fe 5270 and H β indices for the early-type control sample (grey shaded contours), ordinary (red filled circles) and peculiar (red open circles) early-type NEOs based on the stellar population models of Thomas, Maraston & Bender (2003) are shown in Figure 9. Contours of all sample galaxies are also shown as dotted lines for comparison. For the Mg b –Fe 5270 and Mg b –H β plots ((a) and (b), Figure 9), our sample galaxies follow the models reasonably well. The majority of (ordinary) early-type NEOs are old, consistent with an isochrone of 12 Gyr, metal-rich above the solar value, and an over abundance in α -elements, which are the general characteristics of massive early-type galaxies (Rich 1988; Gorgas, Efstathiou

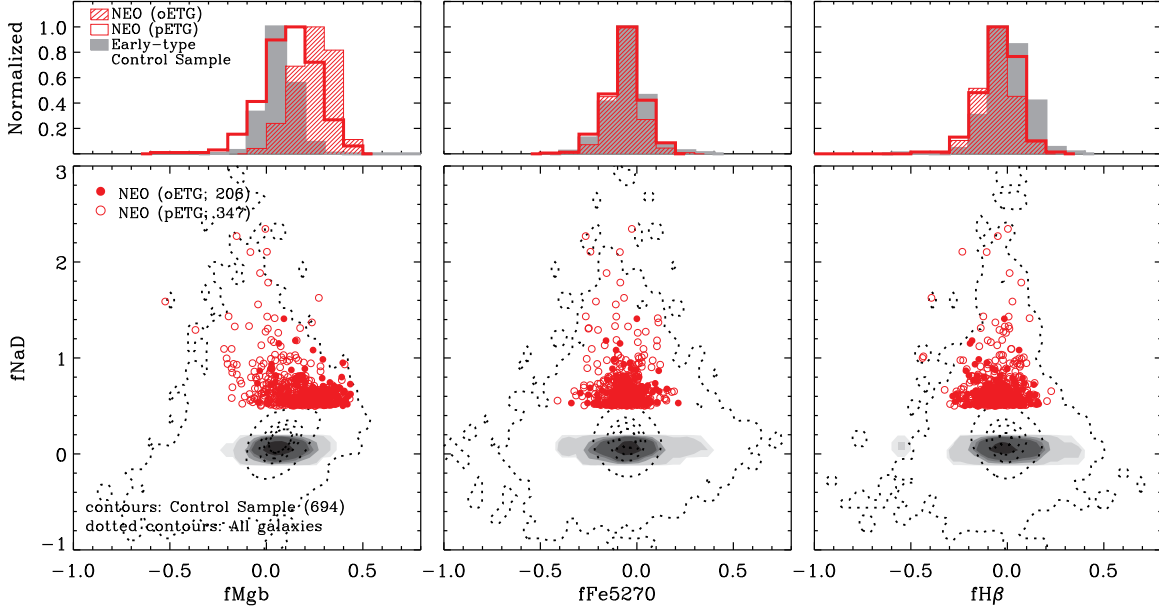


FIG. 7.— *Top*: $Mg\ b$, $Fe\ 5270$ and $H\beta$ excess index histograms for our early-type control sample (grey filled), ordinary (red hashed) and peculiar (red solid) early-type NaD excess objects. *Bottom*: $fNaD$ -excess index plots for the early-type control sample (grey shaded contours), ordinary (red filled circles) and peculiar (red open circles) early-type NEOs. For comparison, the contours of all sample galaxies are shown as dotted lines. A color version of this figure is available in the online journal.

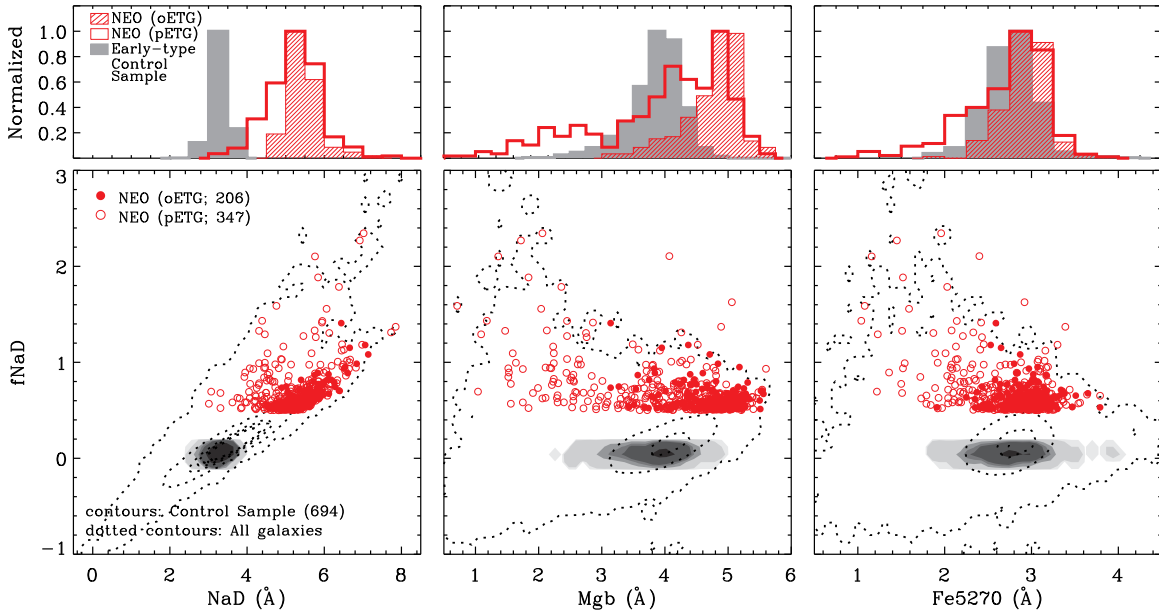


FIG. 8.— *Top*: Histograms of the NaD, $Mg\ b$ and $Fe\ 5270$ line strengths for the early-type control sample (grey filled), ordinary (red hashed) and peculiar (red solid) early-type NaD excess objects. *Bottom*: $fNaD$ -line strength index plots for the early-type control sample (grey shaded contours), ordinary (red filled circles) and peculiar (red open circles) early-type NEOs. The contours of all sample galaxies are also shown as dotted lines for comparison. A color version of this figure is available in the online journal.

& Aragon Salamanca 1990; Worthey, Faber & Gonzalez 1992; Trager et al. 2000; Thomas et al. 2005). However, some peculiar early-type galaxies have stronger $H\beta$ line strengths than the early-type control sample, which is evidence of recent star formation (see e.g. Yi et al. 2005; Kaviraj et al. 2007; Jeong et al. 2007, 2009; Suh et al. 2010; Crockett et al. 2011).

In the NaD-index plots ((c)–(e), Figure 9), the sample galaxies deviate significantly from the model grids. They show enhancement of NaD with respect to $Mg\ b$,

$Fe\ 5270$ and $H\beta$. This behavior indicates that the NaD line strengths of some galaxies, especially at higher NaD strength regions ($Na\ D \geq 4.0\ \text{\AA}$), are difficult to replicate using stellar population models. This brings stellar population models in question, consistent with previous suggestions (e.g. IMF variation and/or overabundance of $[Na/Fe]$), or indicates that the NaD excess may be caused by non-stellar components (e.g. ISM and/or dust).

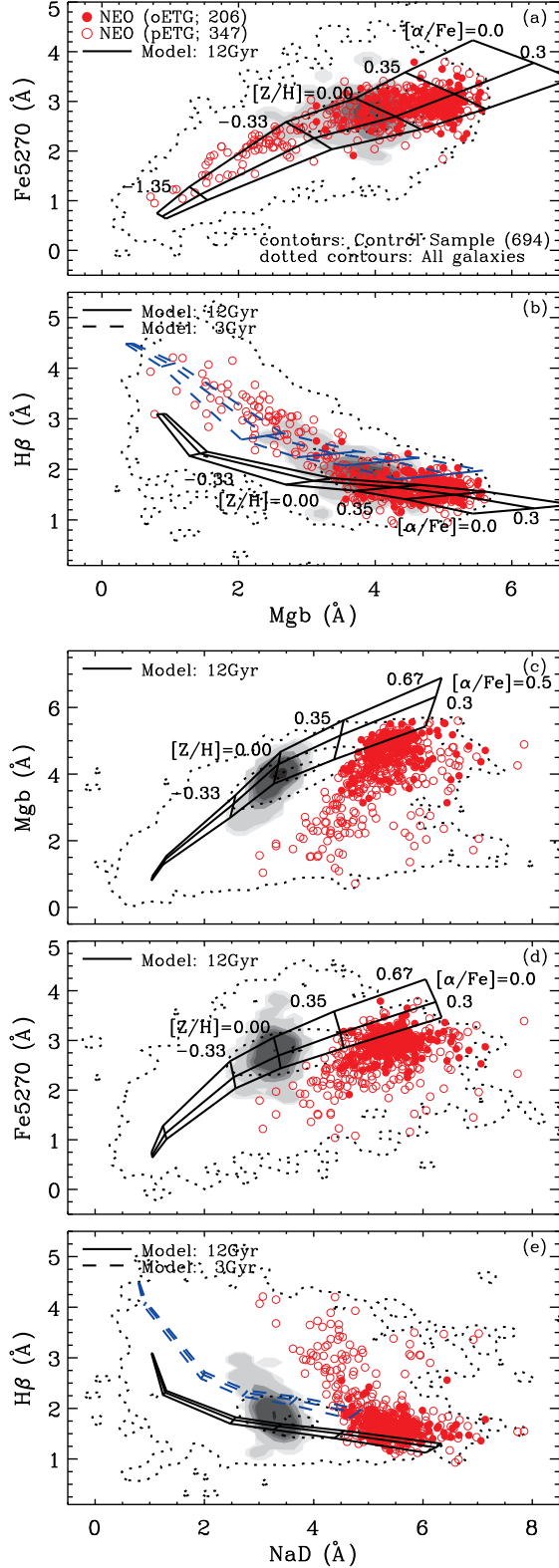


FIG. 9.— Index measurements of our early-type control sample (grey shaded contours), ordinary (red filled circles) and peculiar (red open circles) early-type NEOs compared to the stellar population models of Thomas et al. (2003). For comparison, the contours of all sample galaxies are shown as dotted lines. $Mg\ b$ – $Fe\ 5270$ (a), $Mg\ b$ – $H\beta$ (b), $Na\ D$ – $Mg\ b$ (c), $Na\ D$ – $Fe\ 5270$ (d) and $Na\ D$ – $H\beta$ (e) plots are shown. A color version of this figure is available in the online journal.

3.5. Impact of Interstellar Extinction

It is well known that the NaD index is influenced by the ISM, and dust lanes provide additional absorption in this line. Some studies have reported that dust extinction correlates with NaD line strength (see e.g. Bica & Alloin 1986; Chen et al. 2010; Poznanski, Prochaska & Bloom 2012). We therefore consider the impact of interstellar extinction on the NaD line index to check whether the observed NaD line strength of early-type NEOs can be explained by the ISM and/or dust.

The OSSY catalogue provides two distinct $E(B-V)$ reddening measurements: (1) $E(B-V)_{\text{diffuse}}$, corresponding to a diffuse “screen” dust component that affects the entire spectrum and (2) $E(B-V)_{\text{nebular}}$, associated with a “nebular” component that impacts only the ionized-gas emission, which is known to be generally related to dust features (Sarzi et al. 2006). $E(B-V)_{\text{diffuse}}$ values can be reasonably estimated if the (good-quality) continuum spectra match well with those generated by stellar population models, as is the case for our sample galaxies, whereas $E(B-V)_{\text{nebular}}$ values can be constrained only in the presence of nebular emissions. Moreover, $E(B-V)_{\text{nebular}}$ values depend on our assumption, of an intrinsic Balmer decrement (for more details see OSSY).

In the left panel of Figure 10, we show a comparison of $fNaD$ and the dust extinction values of $E(B-V)_{\text{diffuse}}$ for our sample galaxies using histograms. Early-type control sample (grey filled) and our ordinary early-type NEOs (red hashed) have nearly identical distributions with very little extinction from a diffuse screen dust component. In fact, the uncertainties of our $E(B-V)_{\text{diffuse}}$ measurements are generally so small (less than 0.01 for spectra with an $S/N > 20$, our minimum data quality threshold; see Section 2.2 and Table 1) that our $E(B-V)_{\text{diffuse}}$ measurements are consistent with little or no diffuse dust in our ordinary early-type NEOs, which suggests that their NaD excess may be related to specific aspects of their stellar populations (e.g. different abundance patterns). In contrast, roughly 50% of peculiar early-type NEOs have significant $E(B-V)_{\text{diffuse}}$ values greater than 0.1. This implies that our peculiar early-type NEOs are generally dustier systems than ordinary early-type NEOs and the early-type control sample. This finding is expected because we classified dust lane early-type NEOs as peculiar galaxies.

A comparison of $fNaD$ and $E(B-V)_{\text{nebular}}$ values for our early-type NEOs and early-type control sample galaxies is provided in the right panel of Figure 10. The $E(B-V)_{\text{nebular}}$ values, especially those of the early-type control sample and peculiar early-type NEOs, have skewed distributions with tails toward higher values. The extent of such tails most likely reflects the different incidence of ionized-gas emissions in our early-type subsamples (see Table 3), as expected given the connection between dust features and emission-line regions (Sarzi et al. 2006), whereas the overall similarity of the distributions indicates that nebular dust is not related to NaD excess.

4. PROPERTIES OF LATE-TYPE NaD EXCESS OBJECTS

4.1. Color-Magnitude Relation

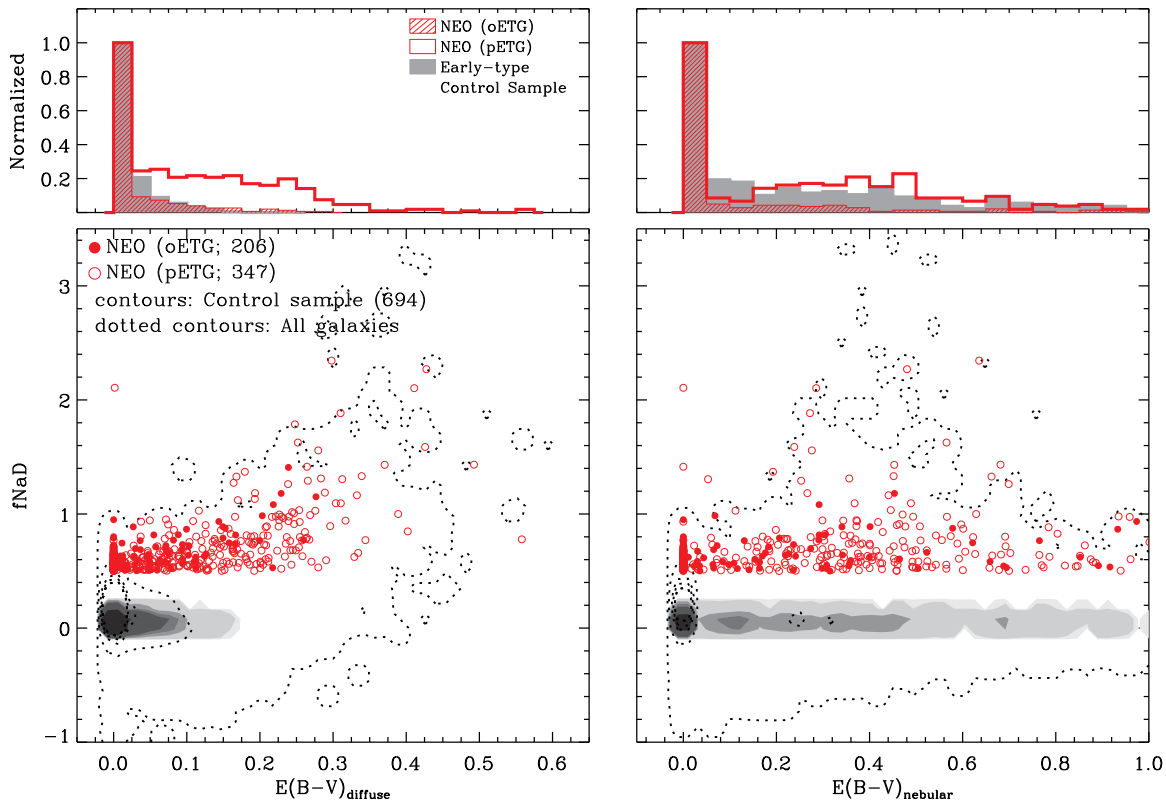


FIG. 10.— *Top*: Distribution of $E(B-V)$ values for the early-type control sample (grey filled), ordinary (red hashed) and peculiar (red solid) early-type Na D excess objects. *Bottom*: $f\text{NaD}-E(B-V)$ plot for the early-type control sample (grey shaded contours), ordinary (red filled circles) and peculiar (red open circles) early-type NEOs. The contours of the sample galaxies are shown as dotted lines for comparison. A color version of this figure is available in the online journal.

It is now common practice to divide galaxy populations on a color-magnitude diagram. Late-type galaxies typically have bluer colors than early-type galaxies and seem to reside in the blue cloud or green valley.

In Figure 11, we present $u-r$ CMR (bottom-left) with M_r (top) and $u-r$ (bottom-right) histograms of our late-type control sample (grey shaded contours and grey filled histogram), ordinary late-type NEOs (blue filled circles and hashed histogram, oLTGs) and peculiar late-type NEOs (blue open circles and solid histogram, pLTGs). A cursory inspection of the plot shows that our late-type NEOs have similar overall ranges of absolute r -band magnitudes and slightly bluer $u-r$ optical color distributions than the late-type control sample, in contrast to early-type NEOs, which are more luminous and optically redder than the early-type control sample. Our late-type NEOs also have a narrower range of M_r , but a wider range of colors, than our early-type NEOs. We note that the difference in peak position of ordinary late-type NEOs may be due to limited number statistics. It is also worth noting that our late-type sample contains a number of red spiral galaxies in the green valley and even in the red sequence.

4.2. Velocity Dispersion and Stellar Mass

The effective velocity dispersion and stellar mass of late-type galaxies are also derived using formulas (1) and (2), respectively. It is important, however, to recognize that these formulas we derived mainly for early-type galaxies, which may lead to measurement errors when

applying them to late-type galaxies.

Figure 12 shows the relationship between the velocity dispersion and stellar mass. The control sample (grey shaded contours) and late-type NEOs (blue filled and open circles) have very similar velocity dispersions and stellar mass distributions (or slightly lower velocity dispersions and smaller stellar masses), unlike the early-type case for which there was a correlation between Na D line strengths and velocity dispersions. We also plot the distributions of velocity dispersion and stellar mass of the late-type control sample (grey filled), ordinary late-type NEOs (blue hashed) and peculiar late-type NEOs (blue solid). We find again that the velocity dispersion and stellar mass distributions of our late-type NEOs are virtually indistinguishable from those of their control counterparts.

4.3. Emission Line Diagnostics: Star Formation and AGN Activity

We begin our spectroscopic analysis by exploring the emission line diagnostic of our late-type galaxies using BPT diagrams (see section 3.3 above).

BPT diagrams for our late-type galaxies are shown in Figure 13. Note again that we only plot galaxies where $[\text{N II}]$, $\text{H}\alpha$, $[\text{O III}]$ and $\text{H}\beta$ lines are detected with $A/N \geq 3$. Black filled circles (left) represent the late-type control sample, while ordinary and peculiar late-type NEOs are indicated by blue filled circles (middle) and blue open circles (right), respectively. To separate galaxies, we use the same demarcation lines as we used for early-type galax-

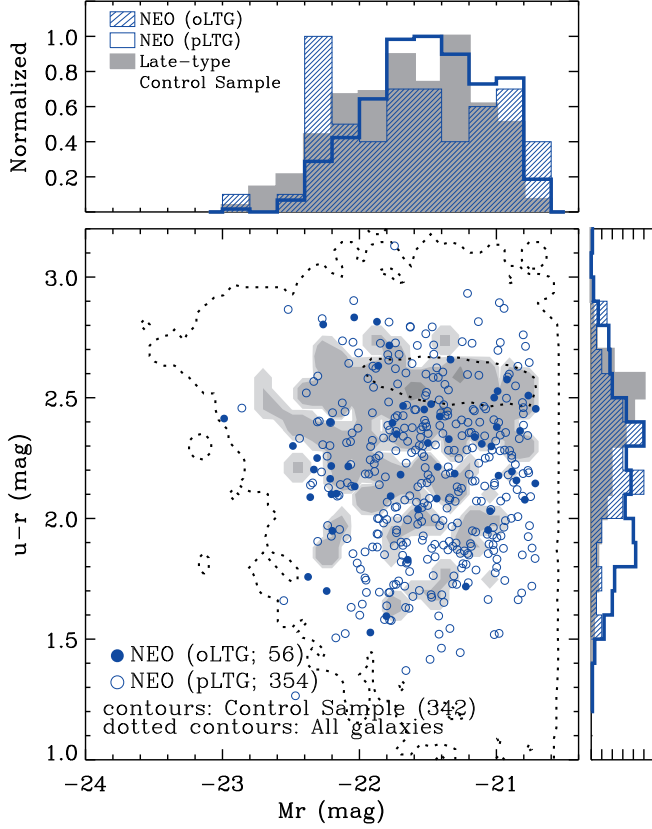


FIG. 11.— Same as Figure 4 but for the late-type control sample (grey filled histogram and shaded contours), ordinary (blue hashed histogram and filled circles, oLTGs) and peculiar (blue solid histogram and open circles, pLTGs) late-type NaD excess objects. A color version of this figure is available in the online journal.

ies (see Section 3.3 and Figure 6). Table 4 summarizes the star-forming, composite and AGN properties of our late-type galaxies.

Interestingly, almost 90% of late-type NEOs show significant emission lines in contrast to early-type NEOs, which are virtually free of emission lines. Star forming galaxies, in particular, are more common in both ordinary and peculiar late-type NEOs. The fractions of late-type NEOs classified as star-forming and composite are larger by factors of 4 and 2, respectively, than those of the late-type control sample, whereas the fractions classified as Seyfert or LINER are slightly lower. Therefore, it appears that the NaD excess in late-type galaxies may be related to phenomena associated with star formation.

4.4. Absorption Line Strengths

We check again the excesses of Mg *b*, Fe 5270 and H β in late-type galaxies by comparing the line strengths between the observations and best-fit model. The bottom panels of Figure 14 show the Mg *b* (left, $fMg\ b$), Fe 5270 (middle, $fFe\ 5270$) and H β (right, $fH\beta$) excess indices, which are calculated using the same procedure as in formula (1), as a function of $fNaD$. Blue filled and open circles represent ordinary and peculiar late-type NEOs, respectively. The dotted contours indicate the distribution of all sample galaxies, while the grey shaded contours indicate the distribution of late-type control sample galaxies. Note that most late-type NEOs have negative

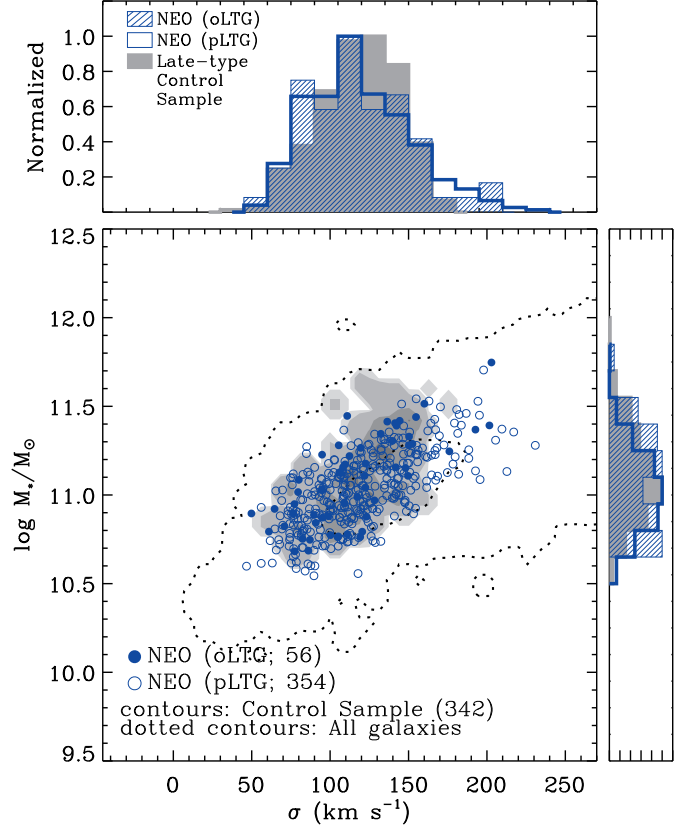


FIG. 12.— Same as Figure 5 but for the late-type control sample (grey filled histogram and shaded contours), ordinary (blue based histogram and filled circles, oLTGs) and peculiar (blue solid histogram and open circles, pLTGs) late-type NaD excess objects. A color version of this figure is available in the online journal.

$fMg\ b$ values, while early-type NEOs tend to have positive $fMg\ b$ values (see Figure 7). This is likely related to enhanced star formation in late-type NEOs, as discussed in Section 4.3 above. Late-type NEOs have $fFe\ 5270$ and $fH\beta$ distributions very similar with those of the late-type control sample.

In the top panels of Figure 14, we also plot the distributions of $fMg\ b$, $fFe\ 5270$ and $fH\beta$. We confirm that the peak positions of the $fMg\ b$ histograms for the late-type control sample (0.05) and late-type NEOs (-0.05) are slightly different. In the cases of $fFe\ 5270$ and $fH\beta$, the distributions of late-type NEOs are virtually indistinguishable from those of their control counterparts (less than 0.03 difference on average), but late-type NEOs show wider deviations in $fFe\ 5270$ than the late-type control sample. For reference, the median values of $fNaD$, $fMg\ b$, $fFe\ 5270$ and $fH\beta$ for our late-type control sample are 0.04 ± 0.03 , 0.05 ± 0.08 , -0.05 ± 0.09 and 0.00 ± 0.09 , whereas those for ordinary late-type NEOs are 0.83 ± 0.52 , -0.04 ± 0.15 , -0.08 ± 0.16 and -0.03 ± 0.07 , respectively.

Figure 15 shows the line strengths of NaD (left), Mg *b* (middle) and Fe 5270 (right) versus $fNaD$. We again see a correlation between $fNaD$ and NaD line strengths, as discussed in Section 3.4. In contrast, the Mg *b* and Fe 5270 line strengths do not show any significant correlations with $fNaD$, but late-type NEOs (blue filled and open circles) tend to have weaker Mg *b* and Fe 5270 line

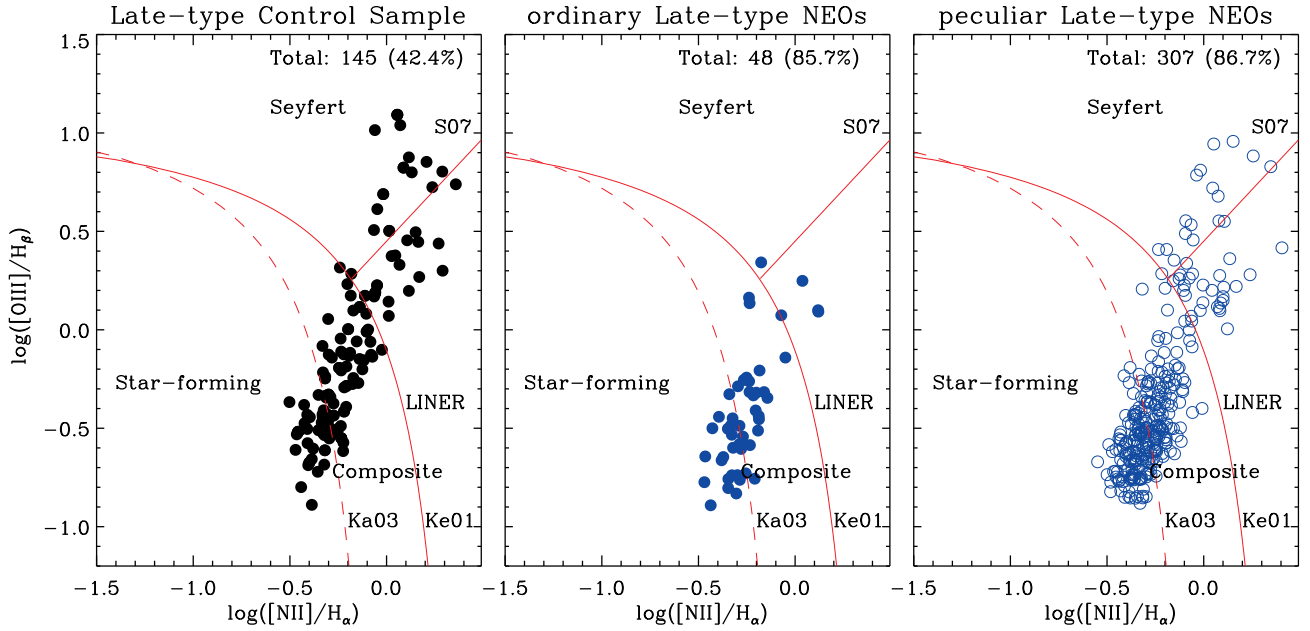


FIG. 13.— Same as Figure 6 but for the late-type control sample (black filled circles, left), ordinary (blue filled circles, middle) and peculiar (blue open circles, right) late-type NaD excess objects. A color version of this figure is available in the online journal.

TABLE 4
RESULTS OF SPECTRAL LINE CLASSIFICATION FOR LATE-TYPE GALAXIES

Classification	late-type control sample	late-type NEOs	oLTGs ^a	pLTGs ^b
Quiescent	57.6% (197)	13.4% (55)	14.3% (8)	13.3% (47)
Strong emission	42.4% (145)	86.6% (355)	85.7% (48)	86.7% (307)
Star-forming	12.0% (41)	41.0% (168)	39.3% (22)	41.2% (146)
Composite	18.7% (64)	33.4% (137)	37.5% (21)	32.8% (116)
Seyfert	5.6% (19)	4.2% (17)	1.8% (1)	4.5% (16)
LINER	6.1% (21)	8.0% (33)	7.1% (4)	8.2% (29)

Notes.

^aordinary late-type NaD excess objects

^bpeculiar late-type NaD excess objects

strengths than the late-type control sample (grey shaded contours) in contrast to the majority of early-type NEOs, which have stronger Mg *b* and Fe 5270 line strengths. In the top panels of Figure 15, the NaD, Mg *b* and Fe 5270 line strength distributions of late-type NEOs and those of their control-sample counterparts are shown; late-type NEOs have stronger NaD line strengths but weaker Mg *b* and Fe 5270 line strengths than their control-sample counterparts.

In Figure 16, we show the absorption line measurements of our late-type galaxies compared to the stellar population models of Thomas et al. (2003). The upper two panels of Figure 16 indicate that our late-type galaxies are very well represented by a coeval (3 Gyr old) sequence of models with various metallicities, while the lower three panels associated with the NaD line strength show that our data deviate from the model grids as in the case of early-type NEOs (see Figure 9). One notable difference is that most late-type NEOs tend to have weaker Mg *b* and Fe 5270 line strengths with enhanced H β strengths, which is further evidence of recent star formation, even though this may not be directly connected to NaD excess.

4.5. Impact of Interstellar Extinction

We consider again the impact of interstellar extinction by comparing the NaD excess index $fNaD$ and the dust extinction values of $E(B - V)_{\text{diffuse}}$ and $E(B - V)_{\text{nebular}}$. We note that both ordinary and peculiar late-type NEOs stand out from the late-type control sample galaxies due to their much larger diffuse screen dust component values (left panel of Figure 17), whereas late-type control sample and late-type NEOs share very similar distributions of $E(B - V)_{\text{nebular}}$ relating to the nebular component (right panel of Figure 17). This suggests not only that the ISM plays an important role in explaining the NaD excess found in late-type NEOs, but also that the ISM contribution to the NaD lines relates only to the diffuse dust component, which also reinforces our previous interpretation of NaD excess in ordinary (dust-free) early-type NEOs. We also further note that the lack of a connection between the nebular dust component and NaD excess is not completely unexpected if we consider that emission-line regions can be quite clumpy, so that only a small fraction of stellar light encompassed by the SDSS spectra is covered.

According to some previous studies (see e.g. Bica &

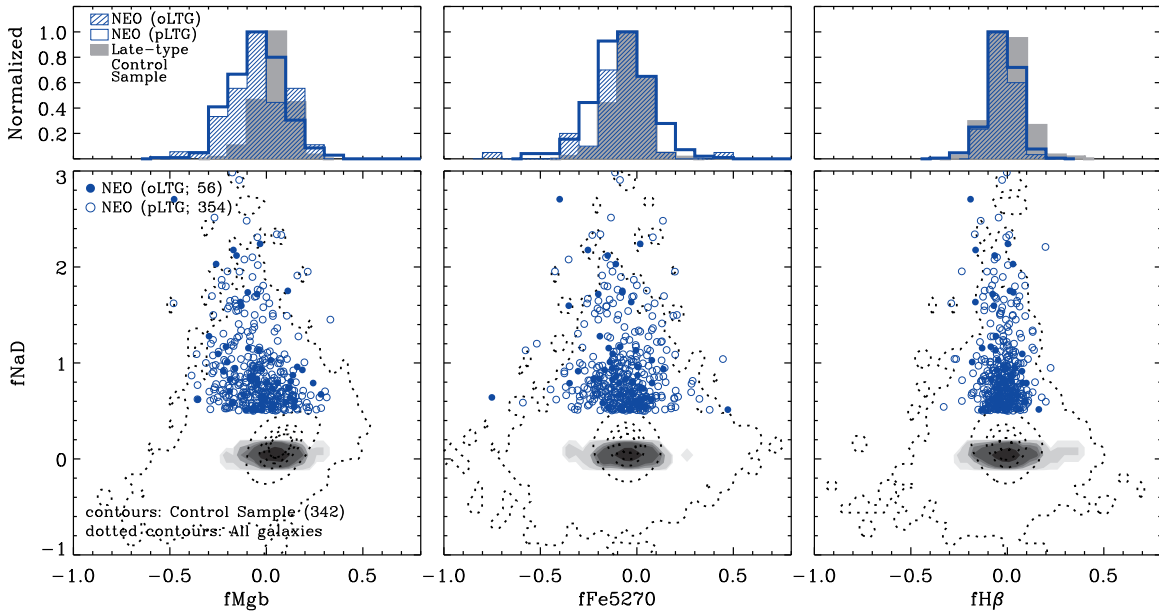


FIG. 14.— Same as Figure 7 but for the late-type control sample (grey filled histogram and shaded contours), ordinary (blue hashed histogram and filled circles, oLTGs) and peculiar (blue solid histogram and open circles, pLTGs) late-type NaD excess objects. A color version of this figure is available in the online journal.

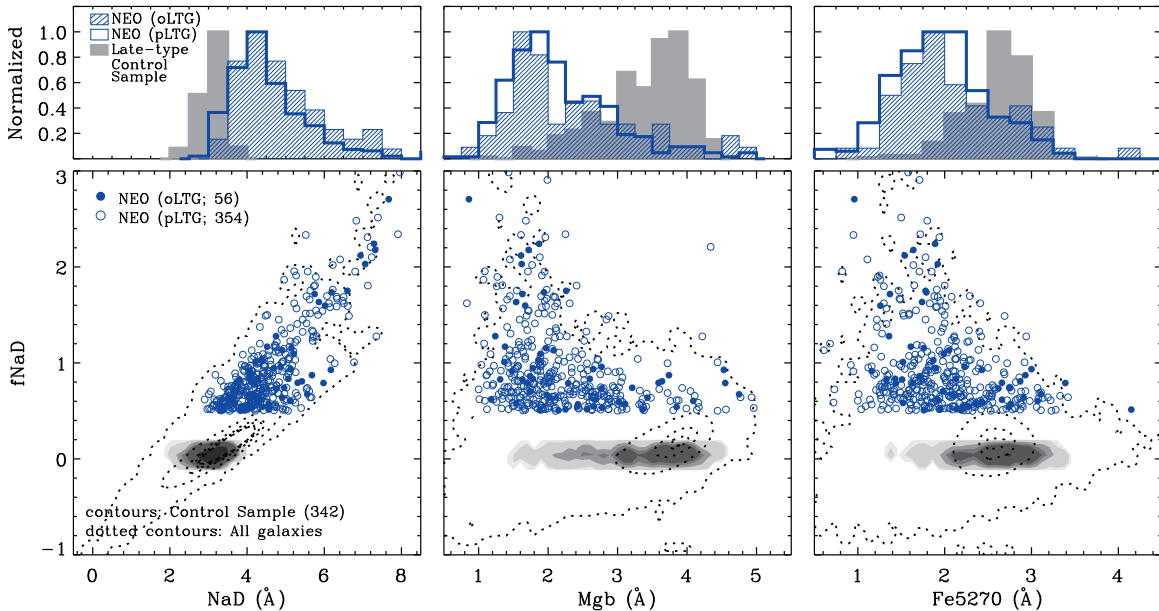


FIG. 15.— Same as Figure 8 but for the late-type control sample (grey filled histogram and shaded contours), ordinary (blue hashed histogram and filled circles, oLTGs) and peculiar (blue solid histogram and open circles, pLTGs) late-type NaD excess objects. A color version of this figure is available in the online journal.

Alloin 1986; Chen et al. 2010; Poznanski, Prochaska & Bloom 2012), the connection between diffuse screen dust extinction and NaD line strength can be valued quantitatively. Adopting the recent calibration of Poznanski, Prochaska & Bloom (2012) for the impact of interstellar absorption on NaD line strength (see their equation 9), the average $E(B - V)_{\text{diffuse}}$ value of ~ 0.3 magnitudes (see Figure 17) observed in our late-type NEOs would be sufficient to explain the main peak shift of $\sim 1 \text{ \AA}$ between the distributions of NaD line strengths for late-type NEOs and that corresponding to the late-type con-

trol sample (see Figure 15). This calibration also allows us to confirm that the impact of the ISM on NaD line strengths in our ordinary early-type NEOs is negligible, even when using a value of 0.01 \AA as an upper limit for $E(B - V)_{\text{diffuse}}$, corresponding to typical uncertainties associated with this quantity (see Section 3.5).

5. DISCUSSION

A number of recent papers exploring Na features that are known to depend on surface gravity have indicated that there is IMF variation among galaxies. To in-

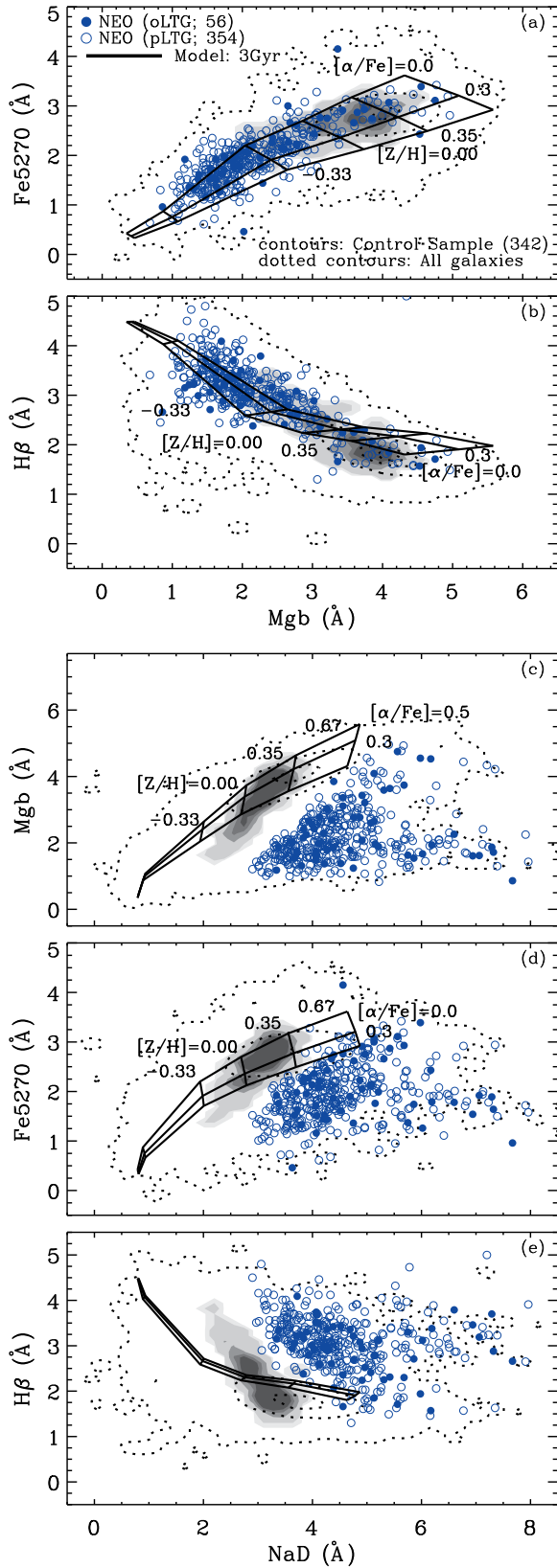


FIG. 16.— Same as Figure 9 but for the late-type control sample (grey filled histogram and shaded contours), ordinary (blue hashed histogram and filled circles, oLTG) and peculiar (blue solid histogram and open circles, pLTG) late-type NaD excess objects. A color version of this figure is available in the online journal.

investigate the nature of NEOs, we selected NaD excess candidates in the redshift range $0.00 \leq z \leq 0.08$ from SDSS DR7 by adopting a new index, $fNaD$. This index quantifies NaD excess by comparing the observed spectrum with the best-fit model spectrum. Roughly 8% (1 603/20 571, $fNaD \geq 0.5$) of galaxies in the sample were classified as NEOs. These galaxies were then identified through direct visual inspection of SDSS images, resulting in a sample of 553 early-type and 410 late-type NEOs. An important goal of this paper was a systematic comparison of the properties of NEOs and those of a control sample based on homogeneous data sets. Note that only 0.5% of galaxies (17/3 461) in the NaD excess range $0.0 \leq fNaD \leq 0.1$ had high velocity dispersions greater than 250 km s^{-1} . This implies that most high velocity dispersion galaxies are classified as NEOs. The results presented in Sections 3 and 4 indicate that the origin of NaD excess may differ considerably depending on galaxy morphology.

The majority of early-type NEOs are optically redder, more luminous, more massive and more likely to be high velocity dispersion systems than early-type control sample counterparts. Furthermore, they are stronger in Mg b and Fe 5270 than their control-sample counterparts, which have roughly solar abundance values (e.g. $[Z/H] \sim 0$ and $[\alpha/Fe] \sim 0$).

Mean observed Mg b and NaD line strengths of the early-type control sample (black open diamond), ordinary early-type NEOs (red filled circle) and peculiar early-type NEOs (red open circle) with a specific stellar population model (black filled square) are shown in Figure 18. The errors correspond to standard deviations. A galaxy with an age of 12 Gyr and solar metallicity (e.g. $[Z/H] = 0$, $[\alpha/Fe] = 0$ and $[Na/Fe] = 0$) with a Salpeter IMF (Salpeter 1955) based on the models of Thomas et al. (2003, see also Lee, Worthey & Dotter 2009; van Dokkum & Conroy 2012) will have NaD and Mg b line strengths of 3.27 and 3.71 Å (black filled square), respectively. These model values are consistent with the observed values of early-type control samples (open diamond).

In contrast, the observed line strengths of early-type NEOs were notably different from the model values (see Figure 9). Given that the NaD index responds more strongly to $[Na/Fe]$ than the IMF and is even influenced by the ISM, one might be tempted to disregard this mismatch. However, it is important, because it provides information about sodium abundance $[Na/Fe]$. To find stellar population models that reproduce the observed line strengths, we explored various factors that may increase the NaD, Mg b and Fe 5270 line strengths based on the models of Thomas et al. (2003, hereafter TMB, 12 Gyr models), Lee et al. (2009, hereafter LWD, 12 Gyr models) and Conroy & van Dokkum (2012, hereafter CV, 13.5 Gyr models).

• α -enhancement effect (green solid and dashed arrows in Figure 18): The Mg b index, which is a well-known tracer of α -elements, changes by 0.59 Å when $[\alpha/Fe]$ varies by +0.3 dex (TMB & LWD, green solid arrow), while Fe 5270 decreases about 0.37 Å with an increasing $[\alpha/Fe]$ (TMB & LWD). The effect of the α -enhancement on NaD, however, is not clear. According to the models of TMB, the NaD feature increases slightly with α -

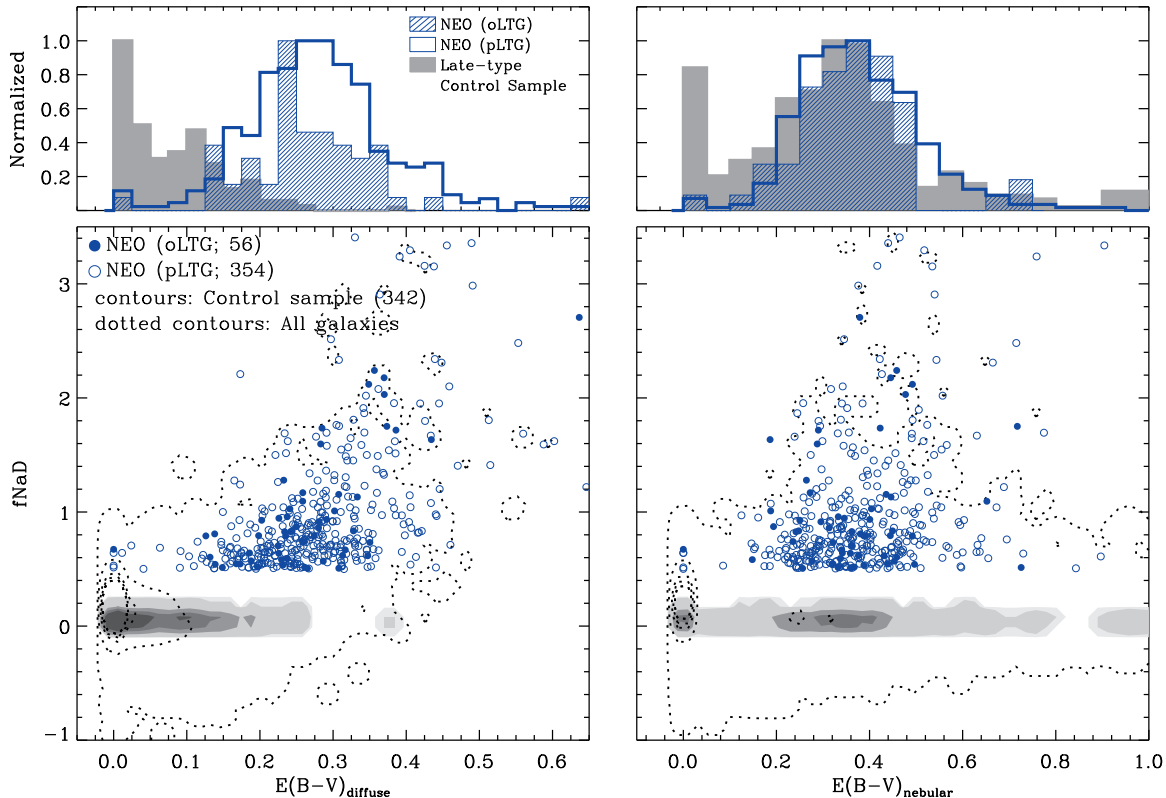


FIG. 17.— Same as Figure 10 but for the late-type control sample (grey filled histogram and shaded contours), ordinary (blue hashed histogram and filled circles, oLTGs) and peculiar (blue solid histogram and open circles, pLTGs) late-type NaD excess objects. A color version of this figure is available in the online journal.

enhancement (see Figures 9c or 16c), whereas in the models of CV & LWD, the NaD line index has weakened about 0.55 \AA on the α -enhancement side ($[\alpha/\text{Fe}] = 0.3$). The green and black dashed curved arrows in Figure 18 represent this tendency. This means that α -enhancement is not conducive to increasing NaD line strength. It is crucial, however, to reproduce the observed Mg b line strength, and it is compatible with our general understanding of massive early-type galaxies (see e.g. Rich 1988; Gorgas, Efstathiou & Aragon Salamanca 1990; Worthey, Faber & Gonzalez 1992; Trager et al. 2000; Thomas et al. 2005).

- Metal effect (violet solid arrow in Figure 18): The Mg b and Fe 5270 indices increase about 0.73 and 0.52 \AA when $[Z/H]$ varies from 0.0 to 0.35 dex. An increase in $[Z/H]$ by 0.35 dex also causes an increase in the strength of NaD by about 1.10 \AA (TMB).

- IMF effect (red solid arrow in Figure 18): The differences in Mg b and NaD line strengths between the Salpeter and $x = -3$ bottom-heavy IMF are only 0.2 and 0.1 \AA , respectively. This implies that IMF variation has a limited impact on Mg b and NaD (CV).

- Na-enhancement effect (blue solid arrow in Figure 18): The NaD line index is known to be particularly sensitive to $[\text{Na}/\text{Fe}]$. At $[\text{Na}/\text{Fe}] = 0.3$, NaD increases about 1.1 \AA (CV).

Given that massive early-type galaxies are known to have an overabundance of α -elements and super-solar total metallicity, it is natural to assume that (ordinary) early-type NEOs have high $[\alpha/\text{Fe}]$ and $[Z/H]$ abundances. Furthermore, our early-type NEOs show strong Mg b and

Fe 5270 line strengths, as described above and in Section 3. Furthermore, the observed Mg b (4.82 \AA) and Fe 5270 (2.98 \AA) line strengths and the peak value of $u-r$ color (2.75 mag) of ordinary early-type NEOs are consistent with the models of TMB ($4.29 \text{ \AA} \leq \text{Mg } b \leq 5.16 \text{ \AA}$ and $2.69 \text{ \AA} \leq \text{Fe } 5270 \leq 3.15 \text{ \AA}$ when $[\alpha/\text{Fe}] = 0.3$ and $0.0 \leq [Z/H] \leq 0.35$) and Yi (2003) ($u-r = 2.74$ when $Z = 0.04$). However, the observed NaD line strength cannot be reproduced with these two assumptions, and the bottom-heavy IMF does not do contribute substantially to increase the NaD strength. We therefore evaluated the hypothesis of enhanced Na abundance.

Most importantly, assuming that our early-type NEOs are “ α -enhanced”, “metal-rich” and “Na-enhanced” without considering IMF variation, we found plausible parameters ($[\alpha/\text{Fe}] \sim 0.3$, $[Z/H] \sim 0.3$ and $[\text{Na}/\text{Fe}] \sim 0.3$) that reproduced the observed Mg b , Fe 5270 and NaD line strengths (see black filled star and red filled circle in Figure 18). A possible criticism is that the hypothesis of Na-enhancement to explain the Na excess is an *ad hoc* assumption. However, several studies have pointed out the presence of Na-enhanced stars (see e.g. Gratton, Sneden & Carretta 2004; Fulbright, McWilliam & Rich 2007). We stress that Na-enhancement also causes an increase in NaI strength and counteracts the effect of the bottom-heavy IMF.

Our analysis does not necessarily rule out the possibility of a bottom-heavy IMF. We simply report that NaD lines, though measured at a much higher S/N ratio than Na I 8190, are too strong in many massive early-type galaxies to be accounted for by the same bottom-heavy

TABLE 5
A SAMPLE OF THE CATALOGUE OF Na D EXCESS OBJECTS.

SDSS object id	RA (J2000)	DEC (J2000)	Redshift	M_r (mag)	$fNaD$	Na D ^a (Å)	$fMg b$	Mg b ^a (Å)	Morphology	BPT class ^b
(1)	(2)	(3)	(4)	(5)	(7)	(8)	(9)	(10)	(15)	(16)
587741490350587994	07:53:54.98	+13:09:16.5	0.0476	-22.33	0.54	5.20	0.27	5.00	oETG	Quiescent
587739115235180592	08:02:15.80	+18:24:08.3	0.0390	-21.77	0.51	5.39	0.26	4.88	pETG	Quiescent
587737809035526294	08:28:06.12	+55:05:55.3	0.0392	-21.80	1.28	4.75	-0.30	1.24	oLTG	Star-forming
587742567860994239	10:42:22.37	+18:08:06.8	0.0518	-21.55	1.69	5.54	-0.05	1.90	pLTG	Liner

(The full table is available in the online version of the paper. A portion of the table is shown here for guidance regarding form and content.)

Notes.

^aObserved line strength from OSSY catalogue.

^bEmission line classification.

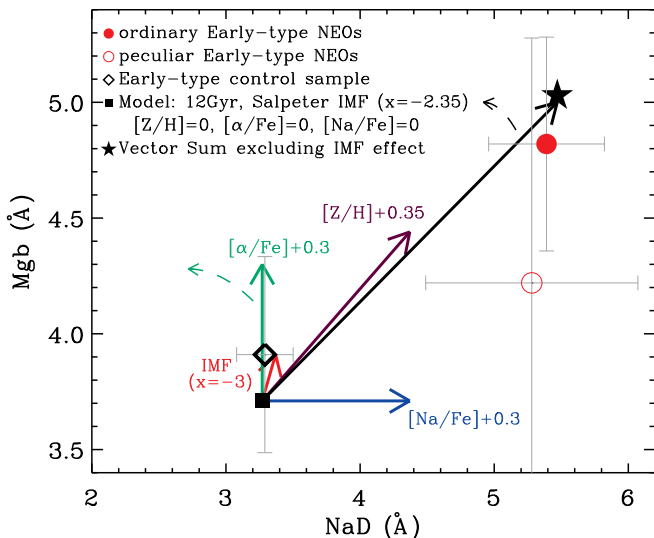


FIG. 18.— Response of Na D and Mg b line indices to changes in the abundance patterns ($[\alpha/Fe]$, $[Z/H]$ and $[Na/Fe]$) and the IMF. The mean observed Na D and Mg b line strengths of the early-type control sample, ordinary and peculiar early-type NEOs are shown by the open diamond, red filled circle and red open circle, respectively. Black filled star represents the vector sum excluding the IMF effect. A color version of this figure is available in the online journal.

IMF models that van Dokkum & Conroy (2010) used to match the Na I 8190 lines. While Na enhancement is discussed here, we have not fully explored its effects on other line indices (e.g. Mg b and Fe 5270). This will be investigated in depth in a forthcoming paper based on new stellar population synthesis models. One more thing to pay attention to is the near-IR (NIR) flux. Worthey, Ingemann & Serven (2011) claimed that such bottom-heavy IMFs would yield redder NIR colors. In another forthcoming companion paper, we will also explore the multi-band (including NIR) photometric properties of NEOs.

ISM and dust could also increase Na D line strength. However, we classified the dust-lane galaxies as peculiar galaxies during the visual inspection stage (see Section 2.4). Notwithstanding that diffuse dust is essentially invisible in optical imaging, our ordinary early-type NEOs are at least free from clumpy dust and emission lines (see Figure 6 and Table 3). Furthermore, there was no correlation between $E(B - V)_{\text{diffuse}}$ values from the OSSY catalogue and $fNaD$, at least for ordinary early-type NEOs, and the $E(B - V)_{\text{diffuse}}$ values of ordinary

early-type NEOs were nearly zero (see Figure 10). This implies that the ISM and/or dust does not enhance the Na D line strength of ordinary early-type NEOs in a significant way. Nevertheless, a study of the presence and properties of the ISM in early-type NEOs is desirable because it is known that a significant fraction of early-type galaxies contain some cool ISM and dust (see e.g. Jura et al. 1987; Knapp et al. 1989).

In contrast, the mechanism for Na D excess in late-type NEOs, including a small fraction of peculiar early-type NEOs that showed very similar trends to the late-type NEOs, appears to be different from that for the majority of early-type NEOs. In contrast to early-type NEOs, enhanced star formation was indicated both by strong H β absorption line strengths and by the higher fraction that were classified as star-forming based on BPT diagnostics. An intriguing property worth discussing here is that late-type NEOs generally have weak Mg b and Fe 5270 line strengths. In that sense, these galaxies could correspond to objects like NGC 3032 and 4150 observed in the course of the SAURON survey (see e.g. de Zeeuw et al. 2002) that experienced recent star formation (Jeong et al. 2009). These characteristics may be caused by young stars (Crockett et al. 2011; Kaviraj et al. 2012). The fact that late-type NEOs have extra young stars is not directly related to Na D line strength, because this would reduce Na D line strength rather than enhance it. However, the presence of star formation and nuclear activity in these galaxies implies the availability of gas and dust, which can impact Na D line strength. Furthermore, we found that our late-type NEOs tended to have larger $E(B - V)_{\text{diffuse}}$ values than the late-type control sample (see Figure 17) in contrast to early-type NEOs.

We thus conclude that early-type (excluding a small fraction of peculiar early-type NEOs) and late-type NEOs have completely different mechanisms underlying their enhanced Na D strengths. The origin of Na D excess in early-type galaxies is not clear yet, but it is clear that early-type NEOs have Na-enhanced populations. The effects of Na-enhancement on individual line strengths will be elucidated in a companion paper. Meanwhile, Na D line strengths in late-type NEOs and a small fraction of peculiar early-type NEOs are highly contaminated by the ISM and/or dust. To facilitate follow-up observations of these exciting objects, we provide a catalogue of all Na D excess objects presented in this paper in Table 5.

ACKNOWLEDGMENTS

The authors thank the anonymous referee for useful comments which led to improvements in the paper and acknowledge support from National Research Foundation of Korea (NRF-2009-0078756; NRF- 2010-0029391) and DRC Grant of Korea Research Council of Fundamen-

tal Science and Technology (FY 2012). Much of this manuscript was written during the visit of SKY to University of Nottingham and University of Oxford under the general support by LG Yon-Am Foundation. This project made use of the SDSS data.

REFERENCES

- Abazajian, K. N., et al. 2009, *ApJS*, 182, 543
 Alloin D., & Bica E. 1989, *A&A*, 217, 57
 Baldwin, J. A., Phillips, M. M., & Terlevich, R. 1981, *PASP*, 93, 5
 Bell, E. F., et al. 2003, *ApJS*, 149, 289
 Bica E., & Alloin D. 1986, *A&A*, 166, 83
 Bruzual, G., & Charlot, S. 2003, *MNRAS*, 344, 1000
 Cappellari, M., & Emsellem, E. 2004, *PASP*, 116, 138
 Cappellari, M., et al. 2006, *MNRAS*, 366, 1126
 Cappellari, M., et al. 2011, *MNRAS*, 413, 813
 Cappellari, M., et al. 2012, *Nature*, 1202, 330
 Carter, D., Visvanathan, N., & Pickles, A. J. 1986, *ApJ*, 311, 637
 Cenarro, A. J., Gorgas, J., Wzdekis, A., Cardiel, N., & Peletier, R. F. 2003, *MNRAS*, 339, L12
 Chen, Y., Tremonti, C. A., Heckman T. M., Kauffmann, G., & Weiner, B. J. 2010, *ApJ*, 140, 445
 Cohen, J. G. 1978, *ApJ*, 221, 788
 Conroy, C., & van Dokkum, P. G. 2012, *ApJ*, 747, 69
 Crockett, R. M., et al. 2011, *ApJ*, 727, 115
 Davé, R. 2008, *MNRAS*, 385, 147
 de Zeeuw, P. T., et al. 2002, *MNRAS*, 329, 513
 Faber, S. M., & French, H. B. 1980, *ApJ*, 235, 405
 Ferreras, I., La Barbera, F., de la Rosa, I. G., Vazdekis, A., de Carvalho, R. R., Falcon Barroso, J., & Ricciardelli, E. 2013, *MNRAS*, 429, 15
 Fulbright, J. P., McWilliam, A., & Rich, R. M. 2007, *ApJ*, 661, 1152
 Gorgas, J., Efstathiou, G., & Aragon Salamanca, A. 1990, *MNRAS*, 245, 217
 Gratton, R., Sneden, C., & Carretta, E. 2004, *ARA&A*, 42, 385
 Graves, G. J., Faber, S. M., & Schiavon, R. P. 2009, *ApJ*, 698, 1590
 Heckman, T. M., Armus, L., & Miley, G. K. 1990, *ApJS*, 74, 833
 Jeong, H., Bureau, M., Yi, S. K., Krajnović, D., & Davies, R. L. 2007, *MNRAS*, 376, 1021
 Jeong, H., et al. 2009, *MNRAS*, 398, 2028
 Jura, M., Kim, D. W., Knapp, G. R., & Guhathakurta, P. 1987, *ApJL*, 312, L11
 Kaviraj, S., et al. 2007, *ApJS*, 173, 619
 Kaviraj, S., et al. 2012, *MNRAS*, 422, 96
 Kauffmann, G., et al. 2003, *MNRAS*, 346, 1055
 Kewley, L. J., et al. 2001, *ApJ*, 556, 121
 Kewley, L. J., Groves, B., Kauffmann, G., & Heckman, T. 2006, *MNRAS*, 372, 961
 Knapp, G. R., Guhathakurta, P., Kim, D. W., & Jura, M. 1989, *ApJS*, 70, 329
 Lee, H.-C., Worthey, G., & Dotter, A. 2009, *AJ*, 138, 1442
 Lehnert, M. D., Tasse, C., Nesvadba, N. P. H., Best, P. N., & van Driël, W. 2011, *A&A*, 532, L3
 O'Connell R. W. 1976, *ApJ*, 206, 370
 Oh, K., Sarzi, M., Schawinski, K., & Yi, S. K. 2011, *ApJS*, 195, 130
 Peterson, R. C. 1976, *ApJL*, 210, 123
 Poznanski, D., Prochaska, J. X., & Bloom, J. S. 2012, *MNRAS*, 426, 1465
 Rich, R. M. 1988, *AJ*, 95, 828
 Saglia, R. P., Maraston, C., Thomas, D., Bender, R., & Colless, M. 2002, *ApJL*, 579, L13
 Salpeter, E. E. 1955, *ApJ*, 121, 161
 Sánchez-Blázquez, P., et al. 2006, *MNRAS*, 371, 703
 Sarzi, M., et al. 2006, *MNRAS*, 366, 1151
 Schawinski, K., et al. 2007, *MNRAS*, 382, 1415
 Spiniello, C., Trager, S. C., Koopmans, L. V. E., & Chen, Y. P. 2012, *ApJL*, 753, L32
 Spinrad H., & Taylor B. J. 1971, *ApJS*, 22, 445
 Suh, H., Jeong, H., Oh, K., Yi, S. K., Ferreras, I., & Schawinski, K. 2010, 187, 374
 Thomas, D., Maraston, C. & Bender, R. 2003, *MNRAS*, 339, 897
 Thomas, D., Maraston, C., Bender, R., & Mendes de Oliveira, C. 2005, *ApJ*, 621, 673
 Trager, S. C., Faber, S. M., Worthey, G., & González, J. J. 2000, *AJ*, 120, 165
 Treu, T., et al. 2010, *ApJ*, 709, 1195
 van Dokkum, P. G. 2008, *ApJ*, 674, 29
 van Dokkum, P. G., & Conroy, C. 2010, *Nature*, 468, 940
 van Dokkum, P. G., & Conroy, C. 2012, *ApJ*, 747, 69
 Worthey, G., Faber, S. M., & Gonzalez, J. J. 1992, *ApJ*, 398, 69
 Worthey, G. 1998, *PASP*, 110, 888
 Worthey, G., Ingermann, B. A., & Serven, J. 2011, *ApJ*, 729, 148
 Yi, S. K. 2003, *ApJ*, 582, 202
 Yi, S. K., et al. 2005, *ApJL*, 619, L111
 Yi, S. K., Lee, J., Sheen, Y.-K., Jeong, H., Suh, H., & Oh, K. 2012, *ApJS*, 195, 22